Constraints on cosmic-ray efficiency in the supernova remnant RCW 86

Renaud, M.; Lemoine-Goumard, M.; Vink, J.; Allen, G.E.; Bamba, A.; Giordano, F.; Uchiyama, Y.; Fermi-LAT Collaboration

DOI
10.1063/1.4772239

Publication date
2012

Document Version
Author accepted manuscript

Published in
High Energy Gamma-Ray Astronomy

Constraints on cosmic-ray efficiency in the supernova remnant RCW 86

M. Renaud*, M. Lemoine-Goumard†,**, J. Vink‡, G. E. Allen§, A. Bamba¶, F. Giordano‖, Y. Uchiyama†† and on behalf of the *Fermi*/LAT collaboration

**LUPM, Université Montpellier 2, CNRS/IN2P3, 34095 Montpellier Cedex 5, France*
†CENBG, Université Bordeaux 1, CNRS/IN2P3, 33175 Gradignan, France
***Funded by contract ERC-StG-259391 from the European Community*
‡Astronomical Institute, Utrecht University, P.O. Box 80000, 3508TA Utrecht, The Netherlands
§MIT Kavli Institute for Astrophysics and Space Research, Cambridge, MA 02139, USA
¶Department of Physics and Mathematics, Aoyama Gakuin University 5-10-1 Fuchinobe, Chuo-ku, Sagamihara, Kanagawa, 252-5258, Japan
‖Dipartimento di Fisica "M. Merlin" dell'Universitá e del Politecnico di Bari, I-70126 Bari, Italy
††W. W. Hansen Experimental Physics Laboratory, Kavli Institute for Particle Astrophysics and Cosmology, Department of Physics and SLAC National Accelerator Laboratory, Stanford University, Stanford, CA 94305, USA

Abstract. Several young supernova remnants (SNRs) have recently been detected in the high- and very-high energy gamma-ray domains, and the nature of this emission is still hotly debated. We have studied the broadband nonthermal emission from one of these SNRs, namely RCW 86, by analyzing $\sim$40 months of *Fermi*/LAT data in the high-energy domain, and the archival X-ray data from several instruments. The derived *Fermi*/LAT upper limits, together with the H.E.S.S. measurements, are incompatible with a standard E_p^{-2} hadronic emission arising from p-p interactions, and can only be accommodated by a particle spectrum harder than $E_p^{-1.8}$. In such hadronic scenario, the total energy in hadrons $\eta_{CR} = E_{CR}/E_{SN}$ is $\sim 0.07\ d^2_{2.5}/\bar{n}_{cm-3}$ (with $d_{2.5} \equiv d/2.5$ kpc and $\bar{n}_{cm-3} \equiv \bar{n}/1\ cm^{-3}$), and the average magnetic field B must be larger than 50 μG in order to significantly suppress any leptonic contribution. On the other hand, the interpretation of the gamma-ray emission by inverse Compton scattering reproduces the multi-wavelength data using a reasonable value for B of 15–25 μG. In this leptonic scenario, we derive a conservative upper limit to η_{CR} of $0.04\ d^2_{2.5}/\bar{n}_{cm-3}$.

Keywords: Supernova remnants (individual: RCW 86), Astronomical observations: γ-ray
PACS: 98.38.Mz, 95.85.Pw

INTRODUCTION

Our understanding of CR acceleration in SNRs mainly relies on the so-called Diffusive Shock Acceleration theory [see *e.g.* 14], commonly invoked to explain several observational lines of evidence for efficient particle acceleration at the SNR forward shocks up to very-high energies. The observed broadband nonthermal emission of individual SNRs offers new insights into the particle acceleration mechanisms at work, given the large panel of multi-wavelength observations available nowadays towards many Galactic SNRs. In particular, recent observations in the high-energy (HE; $0.1 < E < 100$ GeV) and very-high energy (VHE; $E > 100$ GeV) gamma-ray domains have raised several questions and triggered numerous theoretical investigations [*e.g.* 23, 5], as shown by the *Fermi*-LAT [1] and H.E.S.S. [2] observations towards RX J1713.7−3946 [8, 13].

RCW 86 [16] is a 42′-large Galactic SNR in the southern sky. Williams et al. [20] have recently suggested that RCW 86 is likely the remnant of a type Ia SN whose off-center explosion has occurred in a low-density cavity carved by the progenitor system [see also 17]. This scenario would explain the young age (based on its connection with AD 185), and the relatively large distance of RCW 86, which we scale in terms of $d_{2.5} \equiv d/(2.5\ \mathrm{kpc})$ throughout the paper. The general outline of its nearly circular shell is similar at many wavelengths, although significant fine-scale differences have been reported [*e.g.* 15]. In particular, X-ray observations towards RCW 86 have revealed the presence of both thermal and nonthermal emission, with distinct morphologies [*e.g.* 22].

Physical conditions vary greatly along the shell-like structure: slow shocks [$\sim$ 600–800 km s^{-1}, see *e.g.* 9] and relatively high post-shock densities [$\sim$ 1–2 cm^{-3}, see 20] have been measured in the Southwest (SW) and Northwest (NW) regions, while the Northeast (NE) region exhibits much faster shocks [$\sim$ 2700 km s^{-1} and 6000 ± 2800 km s^{-1}, see 18, 10] and low densities [$\sim$ 0.1 cm^{-3}, *e.g.* 21]. In this region, Helder et al. [10] have recently argued that at least 50% of the total pressure is induced by CRs [see also 19]. This measurement, together with the detection of RCW 86 with H.E.S.S. in the VHE domain [3], seem to point towards an efficient CR source. However, complementary HE observations are needed in order to probe the nature of the gamma-ray emission.

DATA ANALYSIS

The LAT is a gamma-ray telescope that detects photons by conversion into electron-positron pairs between 20 MeV and $>$ 300 GeV, as described in Atwood et al. [4]. The analysis used $\sim$40 months of data collected starting August 4, 2008, with the P7 V6 Instrument Response Functions. We first selected the so-called "Source" events with energies greater than 0.1 GeV, and excluded those with zenith angles larger than 100° to minimize contamination from secondary gamma-rays from the Earth's atmosphere.

A spectral-spatial model containing diffuse and nearby point-like sources was produced [see 12, for details], and the parameters were obtained from a maximum likelihood fit to the data using *gtlike*. Based on this spectral-spatial model, we computed the LAT Test Statistic (TS) map of the region containing RCW 86, whose contours are shown in Figure 1. No significant excess is evident in the skymap, apart from a faint excess located near the NE shell of RCW 86, though with a TS of $\sim$ 12 ($\sim$ 2.4 σ for 4 dof) under the assumption of a point-like source. To determine an upper limit on the gamma-ray emission from RCW 86, we added an extended source consistent with the H.E.S.S. observations. In the 0.1 – 1, 1 – 10, and 10 – 100 GeV energy bands, the likelihood ratio test indeed indicates TS $<$ 25. For a fixed spectral index $\Gamma = 2$, we then derived 99.9% CL upper limits (see Figure 2).

We have also re-analyzed the archival X-ray data from *ASCA*/GIS, *XMM-Newton*/EPIC-MOS (see Figure 1, in green) and *RXTE*/PCA, to estimate the nonthermal X-ray emission from the SNR. Details about the data analyses are presented in [12]. The nonthermal spectrum from RCW 86 in the 0.5–25 keV band is shown in Figure 2, along with other available multi-wavelength data, in the radio [*e.g.* 7] and VHE [3] domains.

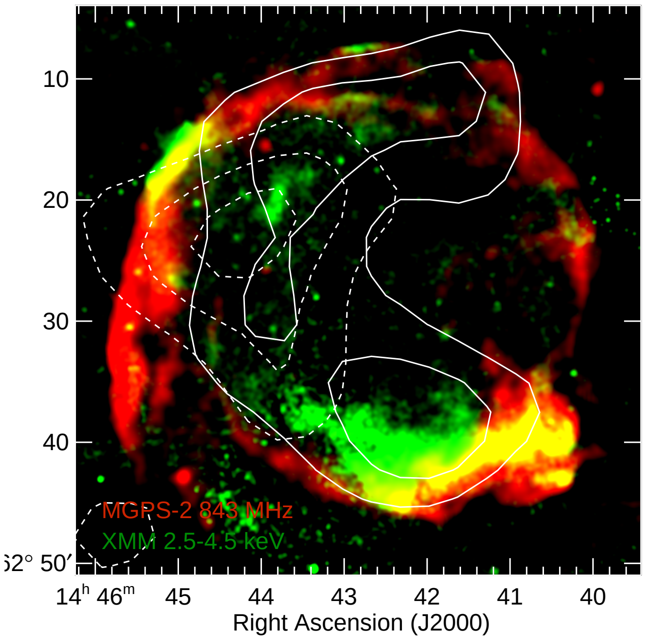

FIGURE 1. MOST (843 MHz, red) and *XMM-Newton*/MOS (2.5-4.5 keV, green) image of RCW 86, with H.E.S.S. [solid lines, 3] and *Fermi*/LAT (dashed lines, TS at E $>$ 1 GeV = 2-4-6) contours overlaid.

DISCUSSION

We aimed at constraining the magnetic field B and the total energy in particles responsible for the nonthermal spectrum of RCW 86, $\eta_{\rm e,p}$ = $\rm E_{e,p}/E_{SN}$ ($\rm E_{SN}$ = 10^{51} erg). We then modeled the π^0-decay gamma-ray emission from p-p interactions [11], and the SC and IC emissions from electrons [6]. The particle spectra were assumed to follow the standard shape $\rm dN_{e/p}/dE_{e/p} \propto E_{e/p}{}^{-\Gamma} \times exp(-E_{e/p}/E_{max,e/p})$. Since any 1-zone model can not account for the morphological difference between radio and X-rays (see Figure 1), we considered two populations of radio- and X-ray-/γ-ray-emitting particles, in the so-called leptonic and hadronic scenarios. For both scenarios, the radio emission is due to SC from an electron population with Γ = 2.2, $\rm E_{max,e} \sim$ 0.2 TeV and $B >$ 10–25 μG, $\eta_{\rm e} <$ (0.5–2.5) $\times$ 10^{-2} $\rm d^2_{2.5}$ [depending on the level of seed photons for the IC emission, see 12], in order to mitigate the IC contribution to the total gamma-ray emission.

In the leptonic scenario, X-/gamma-ray emissions are accounted for with an electron population with Γ = 2, $\rm E_{max,e}$ = 20–25 TeV, B = 15–25 μG and $\eta_{\rm e}$ = (2–4) $\times$ 10^{-4} $\rm d^2_{2.5}$. The estimated *maximal* energy injected into accelerated hadrons is then 4 $\times$ 10^{49} $\rm d^2_{2.5}/\bar{n}_{cm-3}$ erg. In the hadronic scenario, a reasonable fit to the multiwavelength data is found by assuming $B >$ 50 μG, and an electron spectrum with Γ = 1.8, $\rm E_{break,e}$ = 3 TeV (produced by SC cooling), $\rm E_{max,e}$ = 20 TeV and $\eta_{\rm e} \sim$ 6 $\times$ 10^{-5} $\rm d^2_{2.5}$. The associated hadron spectrum, responsible for the VHE emission observed with H.E.S.S. then features $\rm E_{max,p}$ = 20 TeV and a total energy of 7 $\times$ 10^{49} $\rm d^2_{2.5}/\bar{n}_{cm-3}$ erg.

Our B-field estimates for the two scenarios fall within the range of previously reported

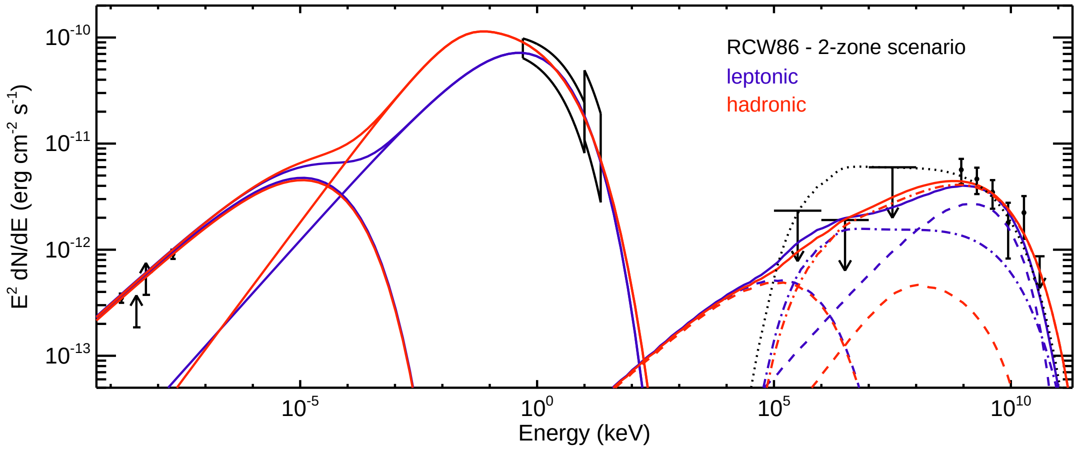

FIGURE 2. Broadband spectral distribution of RCW 86 with the 2-zone leptonic (blue) and hadronic (red) models. Synchrotron [SC], inverse Compton (IC, on CMB only) and π^0-decay spectra are shown as solid, dashed and dash-dotted lines, respectively [see 12]. The black dotted line shows the (excluded) case of π^0 emission from a E^{-2} hadron spectrum with $\eta_p \sim 0.15\ d^2_{2.5}/\bar{n}_{cm-3}$ and $E_{max,p}$ = 100 TeV.

estimates [see 12]. Regarding the CR energy content in RCW 86, our conservative upper limit of $7 \times 10^{49}\ d^2_{2.5}/\bar{n}_{cm-3}$ erg constrains the scenario where $P_{CR} \geq 0.5\ P_{tot}$, as found in the NE region [10], if this were to be applied to the other regions which exhibit higher densities. However, the large uncertainties on the effective CR volume, among others, prevents us from definitively concluding about the acceleration efficiency in RCW 86.

REFERENCES

1. Abdo, A. A., et al. 2011, ApJ, 734, 28
2. Aharonian, F. A., et al. 2007, A&A, 464, 235
3. Aharonian, F. A., et al. 2009, ApJ, 692, 1500
4. Atwood, W. B., et al. 2009, ApJ, 697, 1071
5. Berezhko, E. G., & Völk, H. J. 2010, A&A, 511, 34
6. Blumenthal, G. R., & Gould, R. J. 1970, Rev. Mod. Phys., 42, 237
7. Dickel, J. R., Strom, R. G., & Milne, D. K. 2001, ApJ, 546, 447
8. Ellison, D. C., Slane, P., Patnaude, D. J., & Bykov, A. M. 2012, ApJ, 744, 39
9. Ghavamian, P., et al. 2001, ApJ, 547, 995
10. Helder, E. A., et al. 2009, Science, 325, 719
11. Huang, C.-Y., Park, S.-E., Pohl, M., & Daniels, C. D. 2007, APh, 27, 429
12. Lemoine-Goumard, M., et al. 2012, A&A, 545, 28
13. Li, H., Liu, S., & Chen, Y. 2011, ApJ, 742, L10
14. Malkov, M. A., & O'C Drury, L. 2001, Reports on Progress in Physics, 64, 429
15. Rho, J., et al. 2002, ApJ, 581, 1116
16. Rodgers, A. W., Campbell, C. T., & Whiteoak, J. B. 1960, MNRAS, 121, 103
17. Vink, J., Kaastra, J. S., & Bleeker, J. A. M. 1997, A&A, 328, 628
18. Vink, J., et al. 2006, ApJ, 648, L33
19. Vink, J., Yamazaki, R., Helder, E. A., & Schure, K. M. 2010, ApJ, 722, 1727
20. Williams, B. J., et al. 2011, ApJ, 741, 96
21. Yamaguchi, H., Koyama, K., Nakajima, H., et al. 2008, PASJ, 60, 123
22. Yamaguchi, H., Koyama, K., & Uchida, H. 2011, PASJ, 63, 837
23. Zirakashvili, V. N., & Aharonian, F. A. 2010, ApJ, 708, 965